

Mode Switching-Induced Instability of Multi-source Feed DC Microgrid

Shanshan Jiang, Zelin Sun, Jiankun Zhang, Hua Geng, *Fellow, IEEE*

Abstract—In DC microgrids (DCMGs), DC-bus signaling based control strategy is extensively used for power management, where mode switching plays a crucial role in achieving multi-source coordination. However, few studies have noticed the impact of mode switching and switching strategies on system voltage stability. To fill this gap, this paper aims to provide a general analysis framework for mode switching-induced instability in multi-source DCMGs. First, manifold theory is employed to analyze the stability of the DCMG switched system. Subsequently, the instability mechanism and its physical interpretation are explored. The positive feedback activated by the decreasing DC bus voltage during the switching process leads to instability. Switching strategy may inadvertently contribute to this instability. To improve stability, a novel control method based on mode scheduling is proposed, by adjusting switching strategy and thereby correcting the system trajectory. Finally, both real-time simulations and experimental tests on a DCMG system verify the correctness and effectiveness of theoretical analysis results.

Index Terms—DC microgrid, large-signal stability, mode switching-induced instability, mode scheduling, switching strategy

I. INTRODUCTION

WITH the rapid development of distributed energy resource (DER) and power electronics technology, DCMGs have gained much attention [1]. DCMGs consist of heterogeneous DERs, such as photovoltaic arrays, energy storage systems, etc. The interfacing converters of diverse DERs have different control methods, operating characteristics, and grid-connected positions. Coordination among these converters and DERs is critical to ensure the system power balance and safe operation [2].

For DER coordination and power management, DC bus signaling (DBS), a decentralized strategy, is widely used in DCMGs [3]. Based on local measurements, DBS has the advantage of not requiring real-time communication, low cost, and easy application [4]. DBS strategy works in a limited voltage range, due to the requirements of device safe and efficient operation [5]. When DC-bus voltage is within the range, the converters are controlled collaboratively to share power; when the DC-bus voltage reaches the upper/lower bound, the control methods of converters should be switched to support the DC bus voltage. Therefore, DCMG has several “operational modes”, each of which corresponds to a specific DC bus voltage range and a particular set of control methods

adopted by all converters in the DCMG. “Mode switching” means the transition between operational modes in a DCMG, guided by the energy management strategy, i.e. switching strategy. Such a DCMG is a switched system with different operational modes.

The stability of DCMG switched system is the precondition of its normal operation. In the classification of system stability, small-signal stability analysis (SSA) [6] and large-signal stability analysis (LSA) [7] are two important dimensions. SSA based research is highly developed. It is based on linearizing the system around an equilibrium and the linearized system is then studied by linear tools such as Nyquist stability criterion [8] and eigenvalue analysis [9]. The design of the controller is primarily based on the location of poles and eigenvalues. It is found that constant power loads (CPLs) pose potential instability risks to DCMG for its negative-impedance effect that weakens the system damping and impairs the stability margin [10]. As to LSA, several stability criteria have been obtained, by solving an explicit expression of the approximate region of attraction (ROA) [11], [12], [13]. These stability criteria have been applied in controller designing to stabilize DCMGs [14], [15], [16]. In [14], the mixed potential method is used to regulate the controller parameters to ensure transient stability. In [15], considering ROA dynamics, an active feedback stabilizer is proposed to improve the transient stability of DCMG. In [16], through the Lyapunov method, it is shown that when the controller parameters are large enough, the ROA of system equilibrium can be of the desired size.

The stability of switched systems falls within the category of large-signal stability. However, existing research on large-signal stability primarily focuses on specific operational modes [6], [7], [17], [18]. This focus often overlooks the complexities that arise during the transitions between these modes, which can significantly impact overall system behavior. These transitions can introduce dynamic interactions and instabilities that are not captured when analyzing individual modes in isolation. Specifically, for DCMG switched system, different operational modes exhibit distinct dynamic characteristics. When operational modes switch, the state equation of the system changes, leading to alterations in equilibrium points and ROA, which in turn affect the system’s transient process. However, existing research on LSA overlooks the impact of operational mode switching on system stability and focuses on the stability of individual operational modes [19], which could not fully demonstrate the stability of DCMG switched system. In fact, the stability of switched system is not only influenced by the stability of each operational mode but also critically impacted by the switching strategy [20]. It is

(Corresponding author: Hua Geng)

S. Jiang, Z. Sun, J. Zhang and H. Geng are with Beijing National Research Center for Information Science and Technology, Department of Automation, Tsinghua University, Beijing 100084, China (e-mail: jss23@mails.tsinghua.edu.cn; szl24@mails.tsinghua.edu.cn; zjk_thu@mail.tsinghua.edu.cn; genghua@tsinghua.edu.cn).

worth noting that even if all individual modes remain stable, an unconstrained switching strategy may still cause system instability. Therefore, for the DCMG switched system, it is far from sufficient to merely study the stability of each operational mode. The existing conclusions cannot be directly applied to the study of switched system stability. This gap highlights the need for targeted researches. There is a scarcity of studies on DCMG switched systems, and current stability analysis methods have not adequately addressed this issue.

Under the background of mode switching, the interaction among multi-source has intensified, resulting in the stability of the switched system in multi-source DCMG becoming increasingly prominent. Analyzing its stability and designing stable switching strategies have become critical tasks. To fill this gap, this paper takes a photovoltaic (PV)-battery energy storage system (BESS) with CPL as a typical example, and proposes a general analysis framework and control method, which provides a reference for research on mode switching-induced instability in multi-source DCMGs.

Specifically, three questions are investigated in this paper. The first is how to analyze the switching stability of multi-source DCMG. The second is when mode switching, how the voltage stability of DCMG switched system is affected and what the instability mechanism is. The third is, how to ensure the system stability during mode switching.

To solve these questions, first, when analyzing a multi-source system, sources with similar characteristics can be aggregated into an equivalent source. Consequently, the multi-source DCMG is modeled as a system composed of several representative equivalent sources. Second, to reveal the instability mechanism, manifold theory and ROA are employed to analyze the dynamic behavior of the system during switching process. Thereby identifying factors that affect the system's stability. Finally, a novel control method based on mode scheduling is proposed, specifically, by adjusting switching strategy to guarantee the stability of the switched system.

The main contributions of this paper can be summarized as:

- 1) The large-signal stability of multi-source DCMG switched system is investigated. The analysis method utilizing manifold theory can also be applied to other switched systems.
- 2) Clarifying the mode switching-induced instability mechanism mathematically and physically. It is found that the positive feedback mechanism triggered by DC bus voltage decreasing during the switching process can lead to system instability. Switching strategy may inadvertently exacerbate system instability.
- 3) Propose a novel control method based on mode scheduling, exploring the feasibility of correcting system trajectories and stabilizing the system by adjusting the switching strategy.

The rest of this paper is organized as follows. Section II illustrates the DCMG system studied in this paper. Section III models the DCMG switched system. Section IV conducts the stability analysis and explains the mechanism of instability. Section V proposes the mode scheduling method to improve system stability. Section VI presents real-time simulation

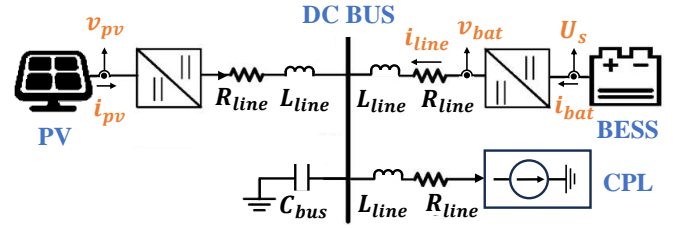


Fig. 1. Topology of a typical 3-machine DCMG.

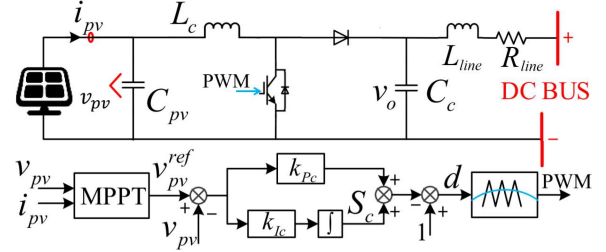


Fig. 2. Structure of the PV unit and its control.

results. Section VII shows experimental results. Section VIII draws conclusions.

II. SYSTEM DESCRIPTION AND MODE DEFINITION

Fig. 1 presents a typical 3-machine DCMG system, which is composed of PV, BESS and CPL. Each source can be regarded as an equivalent or aggregation of multiple devices. The aggregation details can be referenced as [21]. The model is highly simplified, focusing on the external interface characteristics exhibited by these aggregated machines. It does not capture the internal coordination and control processes among the multiple devices. This simplification can be justified as a first principles study to understand the basic instability mechanisms involved in such a multi-source system, which can later be expanded to accommodate other scenarios. PV and BESS are connected to DC bus through the unidirectional and bidirectional boost converters respectively. When PV outputs more (or less) power than CPL consumes, BESS is charged (or discharged).

The structure of the PV unit and its control is shown in Fig. 2. The PV unit usually operates in the maximum power point tracking (MPPT) mode to provide power support. The outer loop adopts perturbation and observation (P&O) algorithm, generating voltage reference value for the inner loop. The inner loop is the proportional integral (PI) based voltage controller.

The structure of the BESS and its control is shown in Fig. 3. Considering the requirements of insulation and device operation, the voltage deviation of DCMG must be limited within a reasonable range. Therefore, BESS adopts two control methods. When the dc bus voltage is operating within the normal range, BESS adopts droop control to realize charge and discharge. When the dc bus voltage reaches the upper or lower limit, BESS adopts constant voltage (CV) control to maintain the bus voltage; in this case, the droop coefficient R_d is set to 0. The outer voltage loop can realize the accurate voltage tracking. The inner current loop can increase the response speed and enhance the system stability.

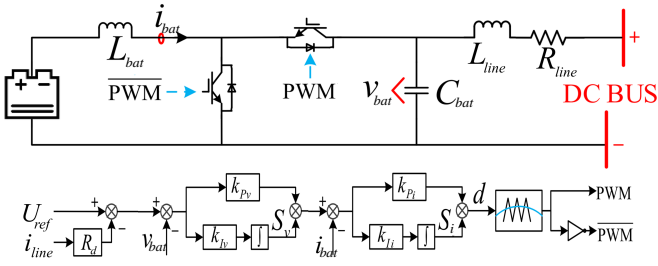


Fig. 3. Structure of the BESS and its control.

The coordination of PV and BESS is achieved through the DBS strategy. The rated DC bus voltage of the DCMG, denoted as V_N , represents the voltage at which only the PV system supplies energy to the CPL. The voltage range for normal operation of the DCMG is $[V_1, V_4]$. In different ranges of DC bus voltage v_{bus} , DCMG works in different modes and the PV-BESS operates in different control methods accordingly. This paper considers several common operational modes of DCMG, which have been mentioned and defined in [19], [22], [23].

- 1) Mode-1 ($V_2 \leq v_{bus} \leq V_1$): v_{bus} is nearing its upper limit. PV output P_{pv} is much greater than the required power of CPL P_{cpl} . PV adopts the MPPT control method. BESS is charged by CV control, which keeps the converter output voltage constant to prevent v_{bus} from over-voltage.
- 2) Mode-2 ($V_N \leq v_{bus} < V_2$): v_{bus} is around the rated value V_N . When $P_{pv} > P_{cpl}$, the excess energy is stored in the BESS. PV adopts the MPPT control method. BESS is charged with droop control.
- 3) Mode-3 ($V_3 < v_{bus} < V_N$): v_{bus} is around V_N . When $P_{pv} < P_{cpl}$, BESS releases power to support stable operation of the system. PV adopts the MPPT control method. BESS is discharged with droop control.
- 4) Mode-4 ($V_4 \leq v_{bus} \leq V_3$): v_{bus} is nearing its lower limit. P_{pv} is much less than P_{cpl} . PV adopts MPPT control method. BESS is discharged by CV control to prevent v_{bus} from under-voltage.

III. MODELING THE DCMG SWITCHED SYSTEM

From the perspective of source and load characteristics, the DCMG multi-machine system consists of power source, voltage source and power load. Considering the equivalent characteristics of the power source and load, the multi-machine system can be simplified to a two-machine system. Each component of the two-machine system is modelled. Then, through singular perturbation theory, the system with different operational modes is transformed into a unified state equation with different parameters. Finally, the DCMG switched system model is constructed.

A. Full-order Modeling

BESS is controlled as a voltage source. The PV unit shows power source characteristics by adopting MPPT control. Considering the equivalent characteristics of PV unit and CPL, the PV unit and CPL are modeled as an equivalent constant

power load (ECPL). The modeling of ECPL and BESS are introduced respectively.

1) *Modeling PV and CPL as ECPL*: PV adopts MPPT control and is regarded as a constant power source. And the PV grid-connected impedance is small enough to be ignored. From the system perspective, the PV and CPL are equivalent to a ECPL, expressed as P_e :

$$P_e = P_{cpl} - P_{pv} \quad (1)$$

The ECPL current $i_e = P_e/v_{bus}$. $P_e > 0$ means ECPL consumes power and $P_e < 0$ means ECPL outputs power.

2) *Modeling BESS*: The control methods of BESS include droop (charging and discharging) control and CV control. CV control can be regarded as a special case of droop control, where the droop coefficient R_d is 0. The reference of the voltage outer-loop control is U_{oref} :

$$U_{oref} = U_{ref} - R_d i_{line} \quad (2)$$

where U_{ref} is the reference voltage of each mode; i_{line} is line current.

According to Fig. 3, the model of BESS can be derived as

$$\begin{cases} \frac{dS_v}{dt} = k_{Iv}(U_{oref} - v_{bat}) \\ \frac{dS_i}{dt} = k_{Ii}(S_v + k_{Pv}(U_{oref} - v_{bat}) - i_{bat}) \\ L_{bat} \frac{di_{bat}}{dt} = U_s - (1-d)v_{bat} \\ C_{bat} \frac{dv_{bat}}{dt} = (1-d)i_{bat} - i_{line} \\ L_{line} \frac{di_{line}}{dt} = v_{bat} - R_{line}i_{line} - v_{bus} \end{cases} \quad (3)$$

where d is the duty ratio. $d = S_i + k_{Pi}(S_v + k_{Pv}(U_{oref} - v_{bat}) - i_{bat})$. S_v and S_i denote the outputs of BESS outer and inner loop integral controllers, respectively; i_{bat} , v_{bat} and U_s represent the BESS output current, BESS capacitive voltage and BESS rated voltage, respectively. L_{bat} , C_{bat} , L_{line} and R_{line} correspond to the filter inductance, filter capacitance, line inductance and line resistance, respectively. k_{Pv} and k_{Iv} are the proportional and integral gains of the voltage loop PI controller, while k_{Pi} and k_{Ii} are those of the current loop PI controller.

Ignoring the minor power loss across R_{line} in Fig. 1, based on the current relationships within the system, the following expression can be derived

$$C_{bus} \frac{dv_{bus}}{dt} = i_{line} - \frac{P_e}{v_{bus}} \quad (4)$$

where C_{bus} is the DC bus capacitance.

From (3) and (4), it can be concluded that the state equation of the DCMG system is 6th order and its state variable $x = [S_v, S_i, i_{bat}, v_{bat}, i_{line}, v_{bus}]^T$.

B. Reduced-order Modeling

Given the two-time-scale characteristic, the dynamics of DCMGs can be classified into slow and fast dynamics, based on their transient velocities. According to this distinction,

the mathematical full-order model can be reformulated into a standard singular perturbed form

$$\begin{aligned}\dot{x} &= f(t, x, z, \epsilon) \\ \epsilon \dot{z} &= g(t, x, z, \epsilon)\end{aligned}\quad (5)$$

where f and g are continuously differentiable, $x \in R_n$ and $z \in R_n$ are the state of the slow subsystem and the state of the fast subsystem, respectively. ϵ denotes a small positive parameter named as perturbation coefficient.

The use of singular perturbation methods is aimed at dividing the system dynamics into two separate time scales, so as to reduce the model order. Specifically, this involves freezing the fast dynamics and degenerating them into static equations. The reduced-order model (ROM) can be obtained by substituting the solutions of these static equations into the slow dynamics equations [24]. Since ϵ is small, the fast transient velocity $\dot{z} = g/\epsilon$ can be much larger than \dot{x} . To address this issue of dual time scales, we can set $\epsilon = 0$, and subsequently, (5) degrades into the following equation

$$\begin{aligned}\dot{x} &= f(t, x, z, 0) \\ 0 &= g(t, x, z, 0)\end{aligned}\quad (6)$$

After time-scale analysis, a 2rd-order ROM can be obtained. $\mathbf{x} = [S_v, v_{bus}]^T$ are the slow dynamic state variables. The ROM can be derived as

$$f = \begin{bmatrix} k_{Iv}(U_{oref} - v_{bat}) \\ \frac{1}{C_{bus}} \left(i_{line} - \frac{P_e}{v_{bus}} \right) \end{bmatrix}\quad (7)$$

$$g = \begin{bmatrix} k_{Ii}(S_v + k_{Pv}(U_{oref} - v_{bat}) - i_{bat}) \\ \frac{1}{L_{bat}}(U_s - (1-d)v_{bat}) \\ \frac{1}{C_{bat}}((1-d)i_{bat} - i_{line}) \\ \frac{1}{L_{line}}(v_{bat} - R_{line}i_{line} - v_{bus}) \end{bmatrix}\quad (8)$$

Since R_{line} is usually small, it can be neglected. The final state equations of the ROM for the DCMG are as follows

$$\dot{\mathbf{x}} = \mathbf{f}(\mathbf{x}) = \begin{bmatrix} k_{Iv}(U_{ref} - R_d i_{line} - v_{bus}) \\ \frac{1}{C_{bus}} \left(i_{line} - \frac{P_e}{v_{bus}} \right) \end{bmatrix}\quad (9)$$

where

$$i_{line} = \frac{U_s}{v_{bus} + U_s k_{Pv} R_d} (S_v + k_{Pv}(U_{ref} - v_{bus})).\quad (10)$$

The accuracy of the ROM will be verified in Section VI.

C. Construction of the DCMG Switched System Model

According to switched system theory [25], a switched system contains a collection of continuous-time subsystems and associated switching strategies orchestrating switching among these subsystems. In DCMG, the ‘‘subsystem’’ mentioned in the above theory is the ‘‘mode’’ defined in this paper. The dynamic evolution process of the switched system is determined by the dynamics of each operational mode and the corresponding switching strategies. The DCMG with multiple

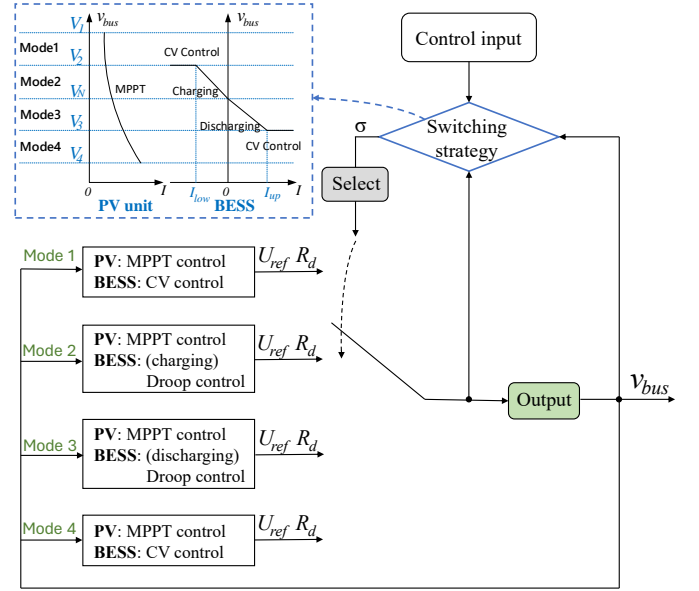


Fig. 4. Diagram of DCMG switched system. The blue dashed box diagram shows the different operational modes of the DCMG, which correspond to the different subsystems of the switching system.

modes can be modeled as a switched system, as shown in Fig. 4. The DCMG switches among different modes according to v_{bus} , so it is state-dependent, i.e. the switching strategy is determined by system state variable v_{bus} . Therefore, the DCMG switched system can be expressed as

$$\begin{aligned}\dot{\mathbf{x}} &= \mathbf{f}_\sigma(\mathbf{x}), \sigma \in \{1, 2, 3, 4\}, \\ \sigma &= \begin{cases} 1 \text{ (Mode-1)}, & \text{if } V_2 \leq v_{bus} \leq V_1 \\ 2 \text{ (Mode-2)}, & \text{if } V_N \leq v_{bus} < V_2 \\ 3 \text{ (Mode-3)}, & \text{if } V_3 < v_{bus} < V_N \\ 4 \text{ (Mode-4)}, & \text{if } V_4 \leq v_{bus} \leq V_3 \end{cases}\end{aligned}\quad (11)$$

where $f_p : p \in S$ is a set of regular functions representing the dynamic equations of modes; $S = \{1, 2, \dots, 4\}$ is an index set that characterizes the discrete states of the system; $\sigma : [0, \infty) \rightarrow S$ is a piecewise constant function taking values in S which represents the switching signal of the system. The switching strategy decides the value of σ .

In the switched system model of DCMG (11), each mode can be expressed in a unified form as (9) and (10), with different parameters:

- In Mode-1 ($\sigma = 1$), $R_d = 0, U_{ref} = V_2$.
- In Mode-2 ($\sigma = 2$), $R_d = R_{d1}, U_{ref} = V_N$.
- In Mode-3 ($\sigma = 3$), $R_d = R_{d2}, U_{ref} = V_N$.
- In Mode-4 ($\sigma = 4$), $R_d = 0, U_{ref} = V_3$.

IV. MODE SWITCHING-INDUCED INSTABILITY ANALYSIS AND MECHANISTIC EXPLANATION

This section studies the stability of DCMG switched system. A transient stability issue is discovered through simulation based on MATLAB/Simulink R2023b. This section analyzes the instability mechanism from the perspective of mathematics

and physics, and explains that switching strategies have an impact on system stability. Then, based on mechanism analysis, theoretical results of system instability are provided.

A. Analysis of the Existence of Equilibrium Points

In Mode-1 and Mode-4, BESS operates under CV control. The system's equilibrium point x_e exists and is unique.

$$\mathbf{x}_e = [S_{ve}, v_{buse}]^T = \left[\frac{P_e}{U_s}, U_{ref} \right]^T \quad (12)$$

Calculate the Jacobian matrix J_e of the ROM at x_e .

$$J_e = \begin{bmatrix} 0 & -k_{Iv} \\ \frac{U_s}{C_{bus}U_{ref}} & -\frac{k_{Pv}U_s}{C_{bus}U_{ref}} \end{bmatrix} \quad (13)$$

where $\det(J_e) = \frac{k_{Iv}U_s}{C_{bus}U_{ref}} > 0$, $\text{tr}(J_e) = -\frac{k_{Pv}U_s}{C_{bus}U_{ref}} < 0$.

According to (13), all the eigenvalues of the system at x_e are positive; therefore, x_e is a stable equilibrium point (SEP) of the system.

In Mode-2 and Mode-3, BESS adopts droop control. The system has two equilibrium points if $U_{ref}^2 - 4P_e R_d > 0$.

$$\begin{aligned} \mathbf{x}_{e1} &= \begin{bmatrix} S_{ve1} \\ v_{buse1} \end{bmatrix} = \left[\frac{P_e}{U_s}, \frac{1}{2} \left(U_{ref} + \sqrt{U_{ref}^2 - 4P_e R_d} \right) \right]^T \\ \mathbf{x}_{e2} &= \begin{bmatrix} S_{ve2} \\ v_{buse2} \end{bmatrix} = \left[\frac{P_e}{U_s}, \frac{1}{2} \left(U_{ref} - \sqrt{U_{ref}^2 - 4P_e R_d} \right) \right]^T \end{aligned} \quad (14)$$

All low-voltage equilibrium points are proved to be unstable in [12]; therefore, x_{e1} is a SEP, while x_{e2} is an unstable equilibrium point (UEP). Simulation results can further validate this conclusion.

B. System Trajectory and Stability Analysis

From the above analysis, it is clear that each mode of the system has a SEP; however, this does not guarantee that the system will remain stable during mode switching. Next, we will further analyze the stability by examining the system's trajectory during these transitions.

Here are some definitions. Before the ECPL step, the DCMG operates at an initial stable equilibrium point (ISEP), and the mode where ISEP resides is the initial mode (IM). After the ECPL step, the system trajectory moves depending on the dynamic equations (9) and the expected SEP (ESEP) can be calculated. The mode where ESEP resides is the expected mode (EM). The sufficient and necessary condition for the system to be stable is that ROA of ESEP covers ISEP. ROA can be obtained using the method developed in [26], which is based on the backward integral along the stable manifold of the UEP. Due to that DCMG has different operational modes in different voltage ranges, state equations vary accordingly, resulting in continuous but non-smooth manifolds and ROA.

Parameters of the DCMG are shown in Table I. In this system, 1kW is defined as the base value for 1 per unit (pu). With the DCMG parameters, the range of P_e of each mode can be selected as follow: In Mode-1, $P_e \in [-1.5\text{pu}, -1.2\text{pu}]$.

In Mode-2, $P_e \in (-1.2\text{pu}, 0]$. In Mode-3, $P_e \in (0, 1.2\text{pu})$. In Mode-4, $P_e \in [1.2\text{pu}, 1.5\text{pu}]$.

In DCMG, the ECPL step is a large disturbance and causes DC-bus voltage variation. In this transient process, DCMG switches operational modes and ROA of ESEP does not necessarily cover ISEP, so the system may suffer instability. The switching strategy has an impact on the stability. Take switching between Mode-1 ($P_e = -1.2\text{pu}$) and Mode-3 ($P_e = 0.1\text{pu}$) as an example. The trajectory of ISEP and ROA of ESEP are shown in Fig. 5 and Fig. 6. The stability of DCMG switching from Mode-1 to Mode-3 is different from the stability switching from Mode-3 to Mode-1. When ECPL power surges and DCMG switches from Mode-1 to Mode-3, ISEP is outside the ROA of ESEP, so instability occurs. However, when ECPL power plunges and DCMG switches from Mode-3 to Mode-1, the ROA of ESEP covers ISEP, therefore the system is stable.

The system stability during mode switching can be determined by plotting ROA and system trajectory. Table II shows 12 typical situations when the mode is switched in pairs. Cases marked with '+' denote ECPL surge, and cases marked with '-' denote ECPL plunge.

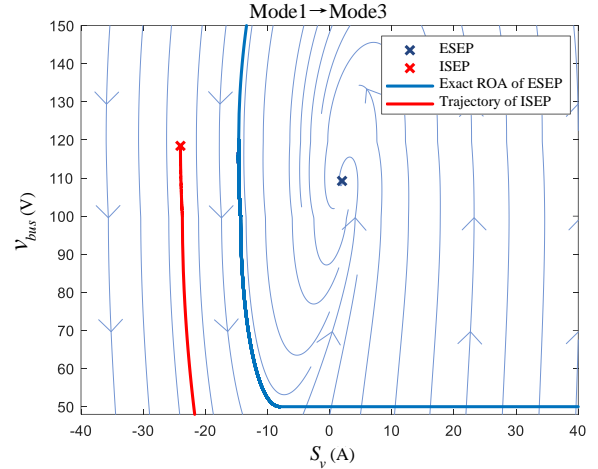


Fig. 5. Trajectory of ISEP and ROA of ESEP: switch from Mode-1 to Mode-3.

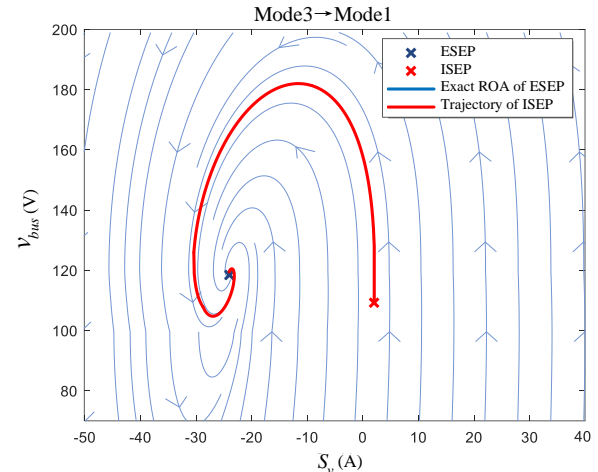


Fig. 6. Trajectory of ISEP and ROA of ESEP: switch from Mode-3 to Mode-1. The ROA extends to the entire upper half-plane.

TABLE I
SYSTEM PARAMETERS

	Parameter	Value
Circuit parameters	R_{line}	0.01Ω
	L_{line}	50μH
	L_{bat}	100μH
	C_{bat}	1mF
	C_{bus}	5mF
	L_c	100μH
	C_c	1mF
	C_{pv}	2mF
	U_s	50V
	I_{low}	-10A
	I_{up}	12A
$v_{bus} - i_{line}$ droop	U_{ref}/R_d	120V/0Ω (Mode1)
		110V/1Ω (Mode2)
		110V/0.83Ω (Mode3)
		100V/0Ω (Mode4)
(PV) PI voltage control loop	k_{Pc} k_{Ic}	0.01 2
(BESS) PI voltage control loop	k_{Pv} k_{Iv}	0.2 4
(BESS) PI current control loop	k_{Pi} k_{Ii}	0.01 20

C. Physical Interpretation of Instability Mechanism

When there is a sudden surge in ECPL, the stability of the system is significantly affected, primarily due to the effect of the positive feedback mechanism. To illustrate the mechanism, we will make some modifications to the equations in the modeling section.

According to the relationship of the currents, i_{line} can be derived as

$$i_{line} = \frac{U_s(S_v + k_{Pv}(U_{ref} - v_{bus}) - k_{Pv}R_d i_{line})}{v_{bus} + U_s k_{Pv} R_d} + \frac{U_s k_{Pv} R_d i_{line}}{v_{bus} + U_s k_{Pv} R_d} \quad (15)$$

where

$$I_{ref} = S_v + k_{Pv}(U_{ref} - R_d i_{line} - v_{bus}) \quad (16)$$

$v_{bus} \approx v_{bat}$. I_{ref} is the reference value of inner loop current.

Rearranged (15), yields

$$i_{line} = \frac{U_s I_{ref}}{v_{bus}} \quad (17)$$

According to (17) and (4), the following expression can be derived as

$$C_{bus} \frac{dv_{bus}}{dt} = \frac{1}{v_{bus}} (U_s I_{ref} - P_e) \quad (18)$$

When the ECPL surges, the reference current I_{ref} cannot be adjusted immediately. As a result, C_{bus} begins discharging to support the increased ECPL demand. This causes the DC bus voltage v_{bus} to drop according to (18). Since the adjustment of I_{ref} is limited by bandwidth constraints, C_{bus} continues to discharge, which in turn causes a further decrease in the bus voltage. At the same time, since the current i_e in the ECPL is inversely proportional to v_{bus} , a decrease in v_{bus}

TABLE II
CASE SETTING FOR THE DCMG SWITCHED SYSTEM

Case	Mode switch	Power variation of ECPL	Transient stability
1+	1→2	-1.5pu→-0.1pu	Unstable
1-	2→1	-0.1pu→-1.5pu	Stable
2+	1→3	-1.2pu→0.1pu	Unstable
2-	3→1	0.1pu→-1.2pu	Stable
3+	1→4	-1.5pu→1.2pu	Unstable
3-	4→1	1.2pu→-1.5pu	Stable
4+	2→3	-0.4pu→0.9pu	Unstable
4-	3→2	0.9pu→-0.4pu	Stable
5+	2→4	-0.1pu→1.2pu	Unstable
5-	4→2	1.2pu→-0.1pu	Stable
6+	3→4	0.1pu→1.3pu	Unstable
6-	4→3	1.3pu→0.1pu	Stable

means that a larger i_e is needed to maintain the same power demand, which further leads to C_{bus} discharging. This positive feedback process exacerbates the decline in v_{bus} and could ultimately destabilize the DCMG system.

The switching strategy further influences the system stability. When ECPL increases, the voltage reference value of the system decreases, resulting in a lower input error of the PI controller in the voltage control loop. This is detrimental to the increase of I_{ref} . Therefore, the switching strategy (11) may hinder BESS from outputting the current ECPL required on time, which has a negative effect on supporting bus voltage.

Based on the above analysis, it is concluded that the large capacitor and high bandwidth help to reduce the impact of positive feedback on system stability to some extent. A larger capacitor means more power storage. Additionally, a high bandwidth corresponds to a short settling time t_s , which is defined as the time for I_{ref} stabilizes within $\pm 5\%$ of the set value. This contributes to improving dynamic response speed. Furthermore, the switching strategy may slow down the DC-bus voltage recovery and harm system stability.

V. PROPOSED MODE SCHEDULING METHOD TO IMPROVE SYSTEM STABILITY

The DC bus voltage is an important state variable reflecting the system stability. When the bus voltage deviates significantly from the rated value, the system becomes unstable. Therefore, when the bus voltage reaches a certain level, it is necessary to adopt measures to correct the system trajectory and prevent further voltage drop. According to the previous section, the switching strategy affects system trajectory and stability. Therefore, by switching the system's operational mode, system stability may be improved. This paper names the method "Mode scheduling".

"Mode scheduling" is defined as: developing system switching strategies offline, monitoring critical state variables online, switching between multiple operational modes based on predefined strategies to correct system trajectory and avoid potential instability, ensuring system behavior being as expected, and ultimately achieving stable operation at the SEP.

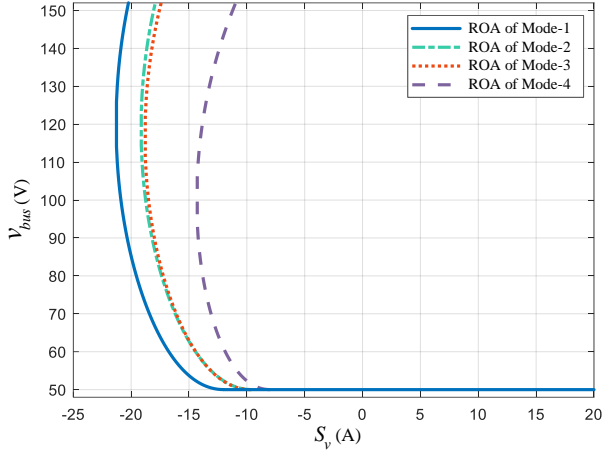


Fig. 7. ROAs of 4 modes when ECPL increases.

Based on the strategy (11), a transitional mode is introduced between IM and EM to lead the system trajectory to ROA. To avoid adding a new mode, the transitional mode can be selected from a predefined mode. One direct method is to select a mode with a large ROA, aiming to cover the ISEP as much as possible. Once the bus voltage surpasses the threshold value, the system switches to the transitional mode, enabling it to adapt to varying operational conditions and requirements.

Fig. 7 depicts the ROA of the system under each mode at the same ECPL. According to Fig. 7, under the same level of ECPL, the ROA of Mode-1 is the largest. Therefore, taking Mode-1 as the transitional mode, it may be possible to change the system trajectory so that ISEP enters the ROA of ESEP. Under the original switching strategy (11), the positive feedback that makes v_{bus} drop to a pretty low level will cause system instability. Therefore, when v_{bus} reaches the threshold, Mode-1 is activated to achieve trajectory adjustment and avoid system instability. The algorithm process is as follows:

- Monitor v_{bus} in real-time.
- If the $v_{bus} \leq V_{min}$, go to step (c). Otherwise, the system works with the switching strategy (11).
- Switch the system to Mode-1.

Here is the adjusted switching strategy based on mode scheduling.

$$\dot{\mathbf{x}} = \mathbf{f}_\sigma(\mathbf{x}), \sigma \in \{1, 2, 3, 4\},$$

$$\begin{cases} \sigma = 1 \text{ (Mode-1), if } V_2 \leq v_{bus} \leq V_1, \text{ or } v_{bus} \leq V_{min} \\ \sigma = 2 \text{ (Mode-2), if } V_N \leq v_{bus} < V_2 \\ \sigma = 3 \text{ (Mode-3), if } V_3 < v_{bus} < V_N \\ \sigma = 4 \text{ (Mode-4), if } V_{min} \leq v_{bus} \leq V_3 \end{cases} \quad (19)$$

The choice of V_{min} can be based on experience or simulation results. In this paper, V_{min} is set to be $90\%V_N$.

Take Case 2+ as an example. When the original switching strategy is adopted, The system trajectory is outside the ROA. The system is unstable. However, when v_{bus} drops below V_{min} , the system switches to Mode-1 for mode scheduling, the trajectory finally arrives at the ESEP. The trajectory of

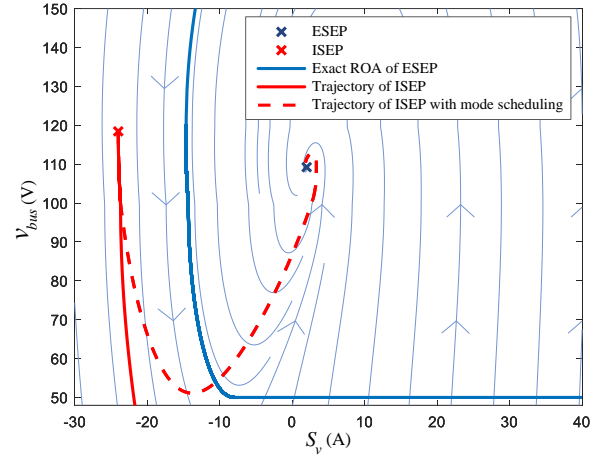


Fig. 8. The adjusted switching strategy of Case 2+ (Switch from Mode-1 to Mode-3): trajectory of ISEP with adjusted switching strategy and ROA of ESEP.

ISEP is shown in Fig. 8. This adjusted switching strategy will also be verified in real-time simulations in Section VI.

It should be noted that the above adjusted strategy provides a new way for improving system stability, but it has a certain scope of application. One premise is that ISEP must fall into the ROA of transitional mode after switching, otherwise it cannot effectively change the system trajectory. In short, this premise limits the magnitude of CPL step. Another premise is that the ROA of ESEP must contain SEP of transitional mode, otherwise the system trajectory cannot be guaranteed to enter the ROA of ESEP. In the scenario discussed in this article, this premise is satisfied.

VI. REAL-TIME SIMULATION VERIFICATION OF THE STUDIED DCMG SYSTEM

To verify the existence of mode switching-induced instability of DCMG, its instability mechanism, and the feasibility of the mode scheduling method, real-time simulation experiments based on MT8020 simulator are carried out. The experimental parameters are shown in Table I.

A. Study 1: Verification for the ROM

By comparing the simulations of the full-order model and the ROM, the accuracy of the ROM has been verified.

For ROM, we perform the same experiment as the full-order model, where the CPL steps from 0.5pu to 1.3pu at $t = 2s$, to observe the transient response of the state variables S_v and v_{bus} , as shown in Fig. 9. When the system is subjected to this disturbance, the full-order model and the ROM exhibit good consistency during the transient process, and share the same SEP. To validate the models' stability under large disturbances, we further increase the CPL from 0.5pu to 1.45pu and compare the instability behaviors of the full-order model and the ROM, as shown in Fig. 10. It is noteworthy that the full-order model exhibits large-signal instability when the CPL increases to 1.4pu , whereas the ROM's critical value is 1.45pu . This difference indicates that the ROM has approximately 3.5% error compared to the full-order model in analyzing

the system's stability boundary. After subsequent analysis and validation, it is found that the error does not affect the stability analysis.

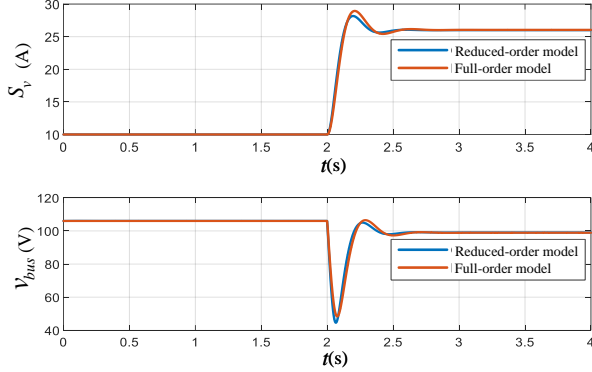


Fig. 9. Comparison between Full-order model and ROM of Mode1: CPL step from 0.5pu to 1.3pu.

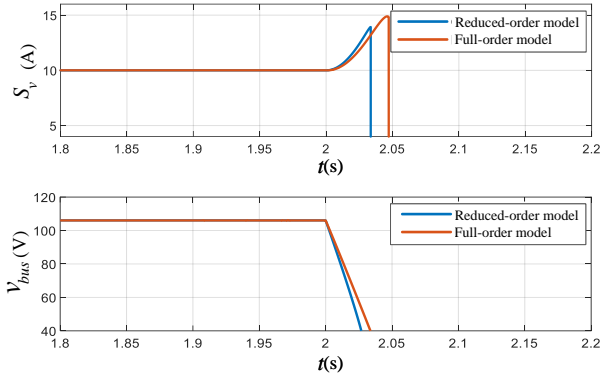


Fig. 10. Comparison between Full-order model and ROM of Mode1: CPL step from 0.5pu to 1.45pu.

B. Study 2: Verification for mode switching-induced instability

According to the theoretical results of Table II, when ECPL plunges, the switched system is stable. In contrast, when ECPL surges, transient stability issues occur. To verify the study, 2 simulation results (e.g., Case 2+/2-) are shown in Fig. 11. In the simulation, the system switches at $t = 2s$.

Among them, the simulation results of Case 2+/2- match the results of the system trajectory and stability analysis in Fig. 5. This indicates that mode switching indeed affects the stability of the DCMG.

C. Study 3: Verification for instability mechanism

To verify the instability mechanism, take Case 5+ switching from Mode-2 to Mode-4 as an example for further illustration. The system switches at $t = 1s$. The parameters of C_{bus} and t_s are changed in simulation. The results are shown in Fig. 12. By observing the waveform of the DC bus voltage, it is found that C_{bus} has a impact on system stability. As the C_{bus} increases, the DCMG system gradually becomes stable. The adjustment of t_s is realized by changing BESS's outer controller parameters. It has been found that under the same CPL step, reducing t_s , thereby increasing the system's response speed, can help to cope with the power disturbances brought to the system by CPL changes to some extent.

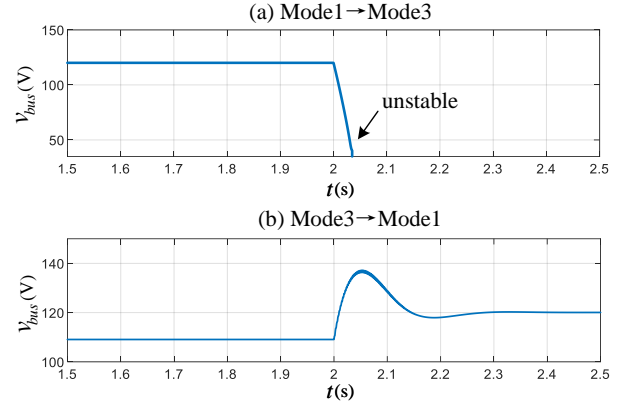


Fig. 11. DC bus voltage simulation results of Case 2+ (Switch from Mode-1 to Mode-3); Case 2- (Switch from Mode-3 to Mode-1).

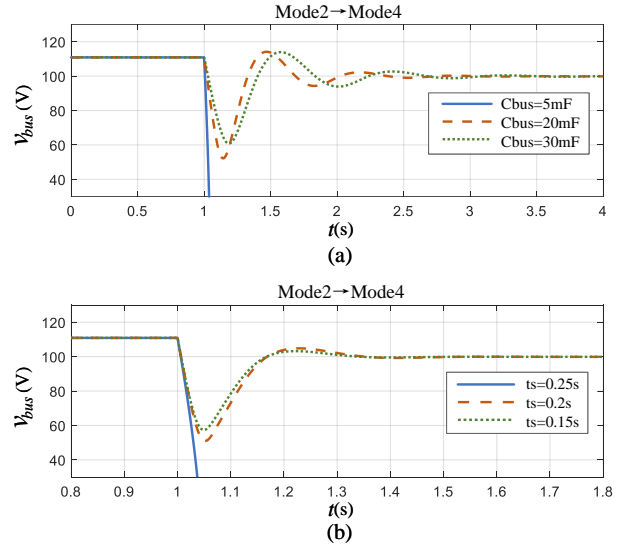


Fig. 12. DC bus voltage simulation results of changing parameters of C_{bus} and t_s in case 5+. (a) The impact of C_{bus} on system stability; (b) The impact of t_s on system stability.

D. Study 4: Verification for mode scheduling method

Take Case 2+, Case 5+ and Case 6+, as examples to verify the feasibility of the mode scheduling method. The CPL steps at $t = 0.5s$. With the strategy (11) the system is unstable as shown by the blue line in Fig. 13. Now, change the switching strategy to (19), the simulation results are shown by the orange line in Fig. 13. It can be found that the system eventually becomes stable, with the adjusted switching strategy. To summarize, the simulation results are in line with the previously conducted theoretical analysis.

VII. EXPERIMENTAL RESULTS

An experimental platform is established to validate the effectiveness of the proposed mode scheduling method, as illustrated in Fig. 14. This platform consists of PV, BESS and CPL, all of which are integrated to form the 110V DCMG. The PV employs a photovoltaic emulator, which is connected to the system through a unidirectional DC converter. The BESS is set up by connecting a programmable DC power supply

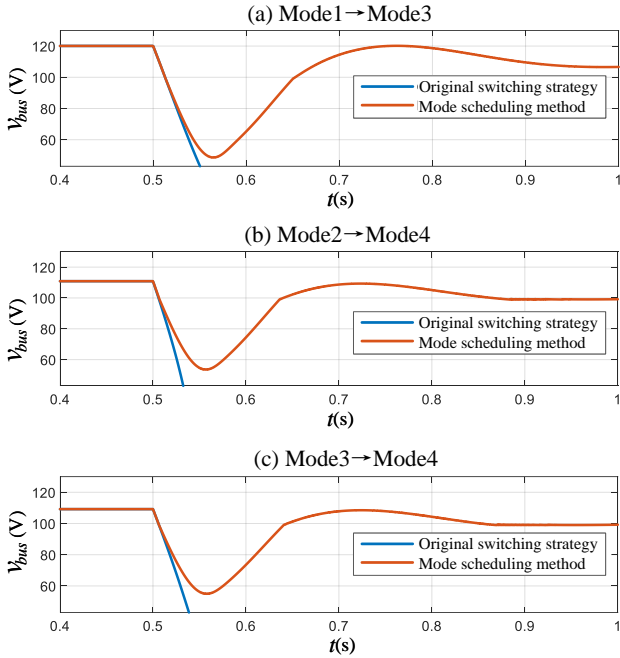


Fig. 13. DC bus voltage simulation results of adjusting switching strategy in case 2+, case 5+ and case 6+. (a) case2+: Mode1 \rightarrow Mode3; (b) case5+: Mode2 \rightarrow Mode4; (c) case6+: Mode3 \rightarrow Mode4.

to the DCMG via a non-isolated bidirectional DC converter. The host computer is used to program the algorithm of the proposed control method and generate PWM signals for real-time control of the two DC converters through the rapid control prototype (RCP) controller (MT1050). The parameters of the photovoltaic emulator and the experimental platform are detailed in Table III and Table I, respectively.

Fig. 15 depicts the experimental waveform of DC bus voltage for Case 2+, Case 5+, and Case 6+, illustrating the effectiveness of the mode scheduling method. With the original switching strategy, mode switching can lead to instability, causing a significant drop in DC bus voltage. In the experiment, a low voltage protection feature is set up. When the bus voltage falls below the 50V input voltage of the bidirectional DC converter, the system triggers a protection mechanism, causing the bus voltage to drop to 0V. By implementing mode scheduling method and modifying the control strategy to equation (19), the bus voltage gradually returns to its nominal level, thereby improving system stability.

VIII. CONCLUSION

TABLE III
PARAMETERS OF THE PHOTOVOLTAIC EMULATOR

Parameter	Value
Maximum power	1689.8W
MPP voltage	34V
MPP current	49.7A
Open-circuit voltage V_{oc}	42V
Short-circuit current I_{sc}	56A

This paper focuses on the mode switching-induced insta-

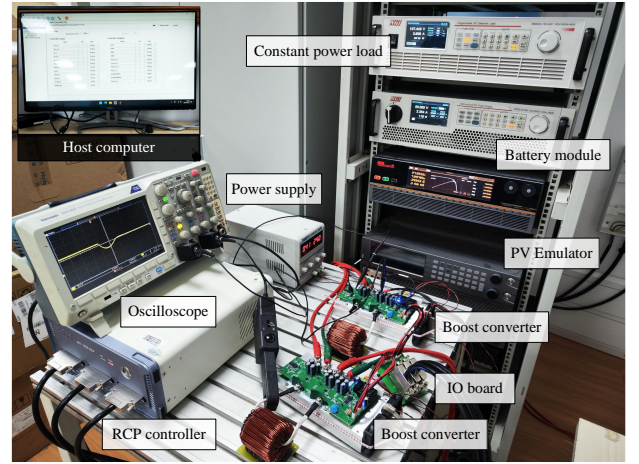


Fig. 14. Photograph of the experimental platform.

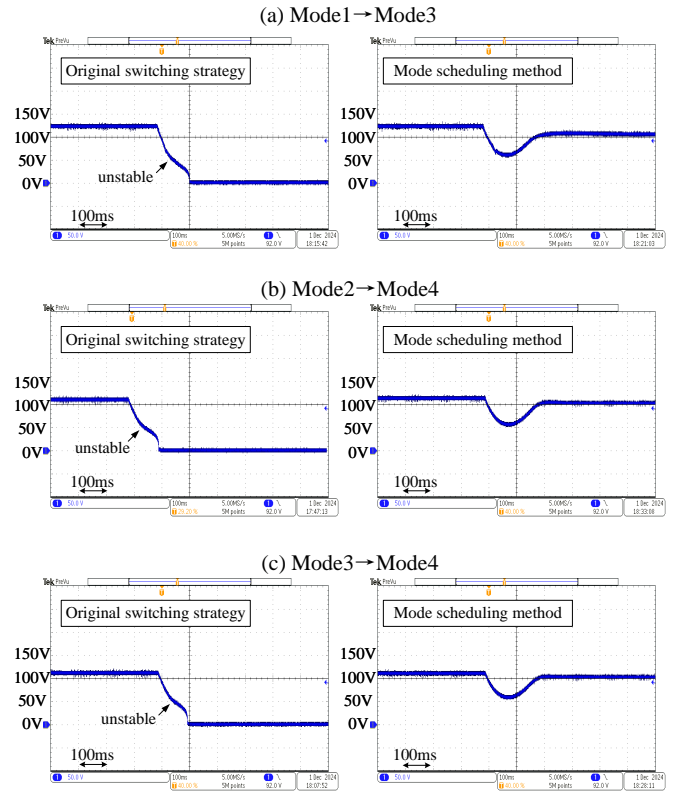


Fig. 15. DC bus voltage experimental results of adjusting switching strategy in case 2+, case 5+ and case 6+. (a) case2+: Mode1 \rightarrow Mode3; (b) case5+: Mode2 \rightarrow Mode4; (c) case6+: Mode3 \rightarrow Mode4.

bility of the DCMG, highlighting the impacts of the switching strategy, and introduces an innovative mode scheduling method to improve system stability. The DCMG operating under various modes, is modeled as a switched system. The instability mechanism is analyzed from both mathematical and physical perspectives, and how switching strategies affect the system stability is illustrated. Subsequently, for scenarios involving unstable mode switching, an adjusted switching strategy is proposed to redirect the system trajectory into ROA of SEP. Based on the findings in this paper, future efforts will concentrate on exploring the mode switching-induced

instability of more complex DCMG switched systems.

ACKNOWLEDGMENT

The authors would like to thank the editor and anonymous reviewers for their insightful comments and suggestions.

REFERENCES

- [1] B. Zhang, F. Gao, Y. Zhang, D. Liu, and H. Tang, "An ac-dc coupled droop control strategy for vsc-based dc microgrids," *IEEE Transactions on power electronics*, vol. 37, no. 6, pp. 6568–6584, 2022.
- [2] H.-J. Yoo, T.-T. Nguyen, and H.-M. Kim, "Consensus-based distributed coordination control of hybrid ac/dc microgrids," *IEEE Transactions on Sustainable Energy*, vol. 11, no. 2, pp. 629–639, 2019.
- [3] A. Garg, N. R. Tummuru, and R. Oruganti, "Implementation of energy management scenarios in a dc microgrid using dc bus signaling," *IEEE Transactions on Industry Applications*, vol. 57, no. 5, pp. 5306–5317, 2021.
- [4] Z. Shuai, J. Fang, F. Ning, and Z. J. Shen, "Hierarchical structure and bus voltage control of dc microgrid," *Renewable and Sustainable Energy Reviews*, vol. 82, pp. 3670–3682, 2018.
- [5] J. Kumar, A. Agarwal, and V. Agarwal, "A review on overall control of dc microgrids," *Journal of energy storage*, vol. 21, pp. 113–138, 2019.
- [6] Z. Liu, M. Su, Y. Sun, W. Yuan, H. Han, and J. Feng, "Existence and stability of equilibrium of dc microgrid with constant power loads," *IEEE Transactions on Power Systems*, vol. 33, no. 6, pp. 6999–7010, 2018.
- [7] Y. Gui, R. Han, J. M. Guerrero, J. C. Vasquez, B. Wei, and W. Kim, "Large-signal stability improvement of dc-dc converters in dc microgrid," *IEEE Transactions on Energy Conversion*, vol. 36, no. 3, pp. 2534–2544, 2021.
- [8] A. P. N. Tahim, D. J. Pagano, E. Lenz, and V. Stramosk, "Modeling and stability analysis of islanded dc microgrids under droop control," *IEEE Transactions on power electronics*, vol. 30, no. 8, pp. 4597–4607, 2014.
- [9] J. Liu, W. Zhang, and G. Rizzoni, "Robust stability analysis of dc microgrids with constant power loads," *IEEE Transactions on Power Systems*, vol. 33, no. 1, pp. 851–860, 2017.
- [10] Z. Liu, R. Liu, Z. Xia, M. Su, X. Deng, X. Zhang, and J. Lu, "Existence and stability of equilibrium of dc micro-grid under master-slave control," *IEEE Transactions on Power Systems*, vol. 37, no. 1, pp. 212–223, 2021.
- [11] F. Chang, X. Cui, M. Wang, and W. Su, "Region of attraction estimation for dc microgrids with constant power loads using potential theory," *IEEE Transactions on Smart Grid*, vol. 12, no. 5, pp. 3793–3808, 2021.
- [12] Z. Liu, X. Ge, M. Su, H. Han, W. Xiong, and Y. Gui, "Complete large-signal stability analysis of dc distribution network via brayton-moser's mixed potential theory," *IEEE Transactions on Smart Grid*, vol. 14, no. 2, pp. 866–877, 2022.
- [13] S. Liu, X. Li, M. Xia, Q. Qin, and X. Liu, "Takagi-sugeno multimodeling-based large signal stability analysis of dc microgrid clusters," *IEEE Transactions on Power Electronics*, vol. 36, no. 11, pp. 12 670–12 684, 2021.
- [14] J. Jiang, F. Liu, S. Pan, X. Zha, W. Liu, C. Chen, and L. Hao, "A conservatism-free large signal stability analysis method for dc microgrid based on mixed potential theory," *IEEE Transactions on Power Electronics*, vol. 34, no. 11, pp. 11 342–11 351, 2019.
- [15] B. Babaiahgari, Y. Jeong, and J.-D. Park, "Dynamic control of region of attraction using variable inductor for stabilizing dc microgrids with constant power loads," *IEEE Transactions on Industrial Electronics*, vol. 68, no. 10, pp. 10 218–10 228, 2020.
- [16] C. Zhang, X. Wang, P. Lin, P. X. Liu, Y. Yan, and J. Yang, "Finite-time feedforward decoupling and precise decentralized control for dc microgrids towards large-signal stability," *IEEE Transactions on Smart Grid*, vol. 11, no. 1, pp. 391–402, 2019.
- [17] F. Chang, X. Cui, M. Wang, W. Su, and A. Q. Huang, "Large-signal stability criteria in dc power grids with distributed-controlled converters and constant power loads," *IEEE Transactions on Smart Grid*, vol. 11, no. 6, pp. 5273–5287, 2020.
- [18] J. Liu, Y. Zhang, A. J. Conejo, and F. Qiu, "Ensuring transient stability with guaranteed region of attraction in dc microgrids," *IEEE Transactions on Power Systems*, vol. 38, no. 1, pp. 681–691, 2022.
- [19] W. Xie, M. Han, W. Cao, J. M. Guerrero, and J. C. Vasquez, "System-level large-signal stability analysis of droop-controlled dc microgrids," *IEEE Transactions on Power Electronics*, vol. 36, no. 4, pp. 4224–4236, 2020.
- [20] H. Lin and P. J. Antsaklis, "Stability and stabilizability of switched linear systems: a survey of recent results," *IEEE Transactions on Automatic control*, vol. 54, no. 2, pp. 308–322, 2009.
- [21] A. A. Nia, N. Shabanikia, and S. A. Khajehoddin, "Droop-based dc microgrids analysis and control design using a weighted dynamic aggregation modeling approach," *IEEE Transactions on Industrial Electronics*, vol. 70, no. 12, pp. 12 299–12 310, 2023.
- [22] K. Sun, L. Zhang, Y. Xing, and J. M. Guerrero, "A distributed control strategy based on dc bus signaling for modular photovoltaic generation systems with battery energy storage," *IEEE transactions on power electronics*, vol. 26, no. 10, pp. 3032–3045, 2011.
- [23] Y. Xia and T. Long, "Chopperless fault ride-through control for dc microgrids," *IEEE Transactions on Smart Grid*, vol. 12, no. 2, pp. 965–976, 2020.
- [24] Z. Ma, Z. Wang, Y. Yuan, and T. Hong, "Singular perturbation-based large-signal order reduction of microgrids for stability and accuracy synthesis with control," *IEEE Transactions on Smart Grid*, 2024.
- [25] Z. Sun, *Switched linear systems: control and design*. Springer Science & Business Media, 2006.
- [26] H.-D. Chiang, M. W. Hirsch, and F. F. Wu, "Stability regions of nonlinear autonomous dynamical systems," *IEEE Transactions on Automatic Control*, vol. 33, no. 1, pp. 16–27, 1988.